Energy Conversion and Management 312 (2024) 118572

Contents lists available at ScienceDirect

Energy Conversion and Management

journal homepage: www.elsevier.com/locate/enconman

Research Paper

Spectral irradiance, ground and crop dynamic reflectance: Key determinants in predicting photocurrent for agrovoltaic systems

M. Barragán Sánchez-Lanuza [a,b], I. Lillo-Bravo [b], G. Egea [c], J.M. Delgado-Sanchez [a,*]

[a] Dpt. Applied Physics I, University of Seville, Ctra. Utrera km 1, 41013 Seville, Spain
[b] Dpt. Energy Engineering, University of Seville, Avda. de los Descubrimientos s/n, 41092 Seville, Spain
[c] Dpt. of Agroforestry Engineering, University of Seville, Ctra. Utrera km 1, 41013 Seville, Spain

ARTICLE INFO

Keywords:
Bifacial
Agrovoltaic
Spectral data
Absolute data
Optical model

ABSTRACT

This research delves into the nuanced dynamics influencing photocurrent generated in bifacial photovoltaic modules within the framework of agrovoltaic applications. Our findings underscore the necessity of using spectral data over absolute values regards to the wavelength dependence for precise energy yield predictions. Particularly, it is demonstrated that the ground reflectance plays a pivotal role. The type of soil (compact or tilled) and crop growth cycle contribute to temporal variations, significantly affecting energy production.

In order to validate the proposed methodology for estimating photocurrent generated by APV systems based on spectral data, we conducted tests in two different irradiance conditions, deliberately chosen for their contrast: clear sky and hazy sky conditions. Experimental measurements were conducted for global, direct, and diffuse irradiance spectral components in both atmospheric scenarios. Additionally, we performed comprehensive spectral reflectance measurements for various soil types and crops throughout an entire growth cycle to depict the temporal variations in these values. It is observed an overestimation in the ratio between front and rear photocurrent generated by the bifacial PV module when the model relies on absolute values of solar irradiance and ground reflectance, compared to utilizing spectral input data. Furthermore, the analysis of absolute values fails to reveal a significant dependence on atmospheric conditions.

In summary, this research discussed the implications of spectral data, geometry and atmospheric conditions, for bifacial PV modules in agrovoltaic applications.

1. Introduction

Bifacial photovoltaic (PV) modules, in contrast to conventional monofacial PV modules, have the capability to absorb solar radiation from both the front and back sides of the PV module [1]. This unique feature allows them to capture not only global radiation but also the diffused and reflected radiation from the Earth's surface. The earliest research on bifacial PV modules dates back to 1960 [2], primarily focusing on crystalline silicon technology. The first commercial product was developed in 1979 specially for the Solar Power Satellite program [3]. Since then, bifacial PV modules have garnered considerable interest in the realm of commercial large-scale PV plants due to their potential to increase energy output while minimizing space requirements compared to conventional PV systems. By 2020, the bifacial technology had captured 17 % of the module market share, a number that has continued to climb, reaching 30 % in 2022 [4,5].

Numerous research studies have examined the influential factors affect the operational efficiency of bifacial PV modules, including solar radiation components (global, direct and diffuse), tilt angle, tracker height, and albedo coefficient. Despite the significance of these factors, a predominant trend among PV system designers involves treating these parameters as absolute values, disregarding spectral information. This practice often stems from the limitations inherent in widely used PV design software such as PVsyst or SAM [6–8]. Notably, Mouhib *et al.* [4] outlined specific albedo coefficient for various ground types, revealing values of 0.334 for light soil, 0.414 for white sand, 0.140 for green grass, and 0.391 for a concrete slab. Their analysis concluded that the selection of white sand as the ground material leads to an optimal energy yield scenario for bifacial PV modules. Furthermore, Asgharzadeh et al. [9] assessed array mismatch production with a ground albedo of 21 %, while Ghenai et al. [10] unveiled a linear relationship between energy yield in bifacial PV modules and the albedo coefficient. In a related study, Jang et al. [11] conducted comprehensive testing on a bifacial PV

* Corresponding author.
E-mail address: jdelgado17@us.es (J.M. Delgado-Sanchez).

https://doi.org/10.1016/j.enconman.2024.118572
Received 3 April 2024; Received in revised form 7 May 2024; Accepted 17 May 2024
Available online 22 May 2024

Nomenclature

R	Absolute reflectivity
APV	Agrovoltaic
f_{DNI}	Angular losses factors of the direct irradiance
f_{DHI}	Angular losses factors of the diffuse irradiance
f_r	Angular losses factors of the reflected irradiance
G_b	Beam irradiance on a horizontal surface
$R_c(\lambda)$	Crop reflectivity
$k_d(\lambda)$	Diffuse fraction correlation
$DNI(\lambda)$	Direct Normal Irradiance
$DHI(\lambda)$	Diffuse Horizontal Irradiance
P_{out}	Electrical output power of PV module
$EQE(\lambda)$	External Quantum Efficiency
FF	Fill factor
$GHI(\lambda)$	Global Horizontal Irradiance
$R_g(\lambda)$	Ground reflectivity
$GHI_R(\lambda)$	Ground-reflected irradiance
$G^{front}(\lambda)$	Irradiance on the front side of the PV module
$G^{rear}(\lambda)$	Irradiance on the rear side of the PV module
V_{oc}	Open-circuit voltage
PV	Photovoltaic
β	PV module tilt angle
ϕ_b	Ratio of the beam irradiance on the tilted surface to that on a horizontal surface
ξ	Relative ratio between front/rear short-circuit photocurrent in the bifacial PV module
ΔJ	Relative difference between absolute and spectral photocurrent
J_{sc}	Short-circuit photocurrent
J_{sc}^{front}	Short-circuit photocurrent in the front side of the bifacial PV module
J_{sc}^{rear}	Short-circuit photocurrent in the rear side of the bifacial PV module
$R(\lambda)$	Spectral reflectivity
$G_{d,tilt}$	Total tilted diffuse irradiance
$F_{i,j}$	View factor coefficients

system, evaluating various operation conditions including the choice of reflecting material, vertical and tilted orientation, and temperature mismatch. However, their findings lacked spectral information pertaining to irradiance or the material properties of the reflecting surfaces. Similarly, Baghel et al. [12] conducted a thorough performance evaluation of a bifacial PV system, optimizing the tilt angle and albedo coefficient using simulation and experimental data collected in India. Also, Sun et al. [13] developed a concise anisotropic model for bifacial PV modules, considering different incident angles and ground reflection conditions, but neither of these studies accounted for any spectral values in the analysis.

Nonetheless, it is imperative to consider the influence of the spectral dependence of solar irradiance and ground surface reflectivity in order to accurately assess the performance of bifacial PV modules, particularly when comparing various boundary conditions [14]. The spectral impact on bifacial PV modules is of heightened significance compared to conventional crystalline silicon PV modules due to the independent interactions of different solar radiation components (global, direct, and diffuse) with the surrounding environment and the PV system, with these interactions being inherently spectrally dependent (Fig. 1). Despite the significance of this factor, only a limited number of studies have utilized spectrally resolved data to investigate the performance of bifacial PV modules. Tonita et al. [15] investigated the correction of spectral albedo mismatch on bifacial PV modules and their energy

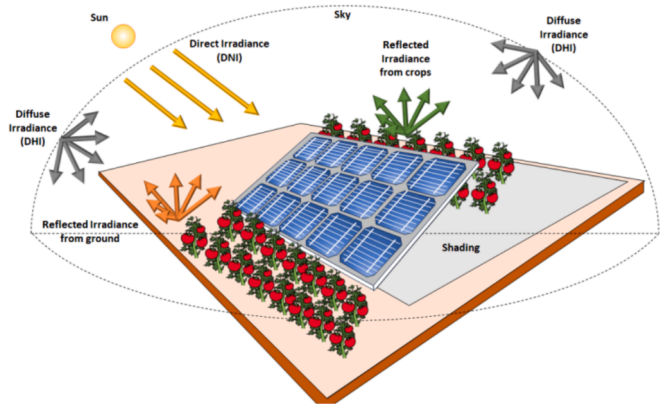

Fig. 1. Bifacial PV system installed on a non-uniform ground covered by crops and soil.

output prediction. Additionally, Riedel-Lyngskaer et al. [16] analyzed experimental data of bifacial PV systems obtained with different spectroradiometers and pyranometers, finding spectral impacts ranging from 0.98 to 1.20. Furthermore, Monokroussos et al. [17] validated an optical model designed to define the spectral irradiance on the rear side of bifacial PV modules under standard test conditions.

One of the most promising applications for bifacial PV modules lies in agrovoltaic (APV) systems. However, in this particular design, heightened precision is imperative for photocurrent generation, and later for the energy yield model. This necessity arises from the intricate interplay of spectral reflections within the adjacent components, such as the vegetation and soils, and it is crucial to consider that both components modify their optical properties over time. So, considering both optical properties as absolute and constant oversize the energy generation estimated in the PV system. The APV concept was originally developed by Goetzberger and Zastrow [18], elucidating that elevating PV modules to a sufficient height ensures the uniform distribution of irradiance on the ground throughout the day, thereby facilitating efficient plant growth. However, new agricultural techniques have undergone significant development in recent years, leading to the classification of APV systems into three main types. The first involves alternating rows of crops and PV strings in an open field. In contrast, the other two configurations entail installing PV modules above the crops, either as the rooftop covering for greenhouse or by mounting the PV modules in an open-air setting [19].

So, the primary advantage of APV systems lies in the potential augmentation of dual land use, thereby mitigating the environmental impact of expansive PV system within society [20]. Dupraz et al. suggested that land use efficiency could be enhanced to 70 % through the implementation of APV systems. This indicates that at least 1.7 times more land would be required to achieve the benefits from individual solar energy generation and conventional agricultural activities [21]. Nonetheless, the increased installation expenses associated with PV modules, inverters, and trackers on agricultural land might lead to higher crop prices, underscoring the significance of mitigating yield losses in APV systems [22].

The fundamental hypothesis underlying this system posits that certain vegetables can withstand partial shading, thereby resulting in a dual benefit of controlling water consumption through reduced soil evaporation and optimizing plant transpiration [23–25]. The identification of crops compatible with PV module shading is pivotal for optimizing the performance of any APV system. Interactions between radiation and plant physiology, alongside other limiting factors for crop

production, are central considerations. Certain vegetables exhibit tolerance to partial shading and can be strategically planted beneath PV modules (Fig. 2a). Conversely, other plant species are recommended to be positioned in the gaps between PV modules in each array (Fig. 2b). These options have a critical influence in the optical model for the photocurrent estimation of the bifacial PV modules installed on the APV system. The selection criteria for these placements revolve around ensuring that the presence of PV modules does not adversely impact their photosynthetically active radiation (PAR) [26–28]. For an in-depth exploration of the environmental factors influencing crop dependence, a comprehensive review is available in [29].

Among the various PV technologies available in the market, bifacial PV modules stand out as one of the most advantageous options for APV applications, either large-scale systems or greenhouses [30,31]. Nevertheless, the accurate prediction of photocurrent in bifacial PV modules installed in APV systems incorporating these modules encounters inherent complexities. Specifically, the diffuse irradiance reaching from the rear surface of the PV module is contingent upon the ground condition (whether it be soil or vegetation) [32]. The non-uniformity of solar radiation on the rear surface of the bifacial PV modules stands as one of the most critical limiting factors. This non-uniformity is heavily contingent upon module elevation, particularly pronounced under conditions of non-uniform irradiance, which are prevalent in APV systems [33]. Furthermore, crop growth stage exerts a notable influence on the type of surface reflection, encompassing Lambertian reflection, specular reflection, directional diffuse reflection, or diffuse retro-reflection.

An additional intricacy that is often overlooked in photocurrent predictions of this nature pertains to the incident angle dependence and the shadowing evolution in the bare soil or crop zone, affecting the reflected diffuse irradiance on the rear side of the bifacial PV module. This issue can be solved using the concept of view factors, typically not integrated into conventional predictions [34]. They rely on the basic principle of conservation of radiation, aiming to estimate the fraction of irradiance reflected from neighboring surfaces or the ground to the rear side of a bifacial PV module through geometric considerations. It is essential to consider the view factor in APV systems, as it profoundly influences the spatial distribution of shading and the result homogeneity of the reflected irradiance, thereby impacting the overall system performance. As such, a comprehensive understanding of the dynamic interplay between ground conditions, crop growth phases, and the view factor is indispensable for refining photocurrent estimation models in bifacial APV systems. However, in our experience, there are no previously published articles analyzing the dynamic effect of crop growth and its impact on the reflectivity to evaluate the performance of bifacial PV modules.

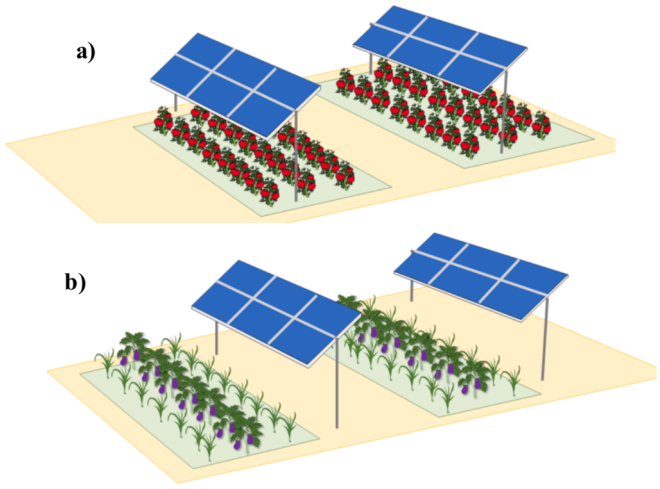

Fig. 2. Different APV design: a) vegetables exploits the shading conditions under PV modules to improve their growth conditions; b) crops are placed between arrays to get maximum irradiance.

It has been previously pointed out the relevance of albedo characterization to predict the performance of APV systems. Moreover, albedo depends on the spectral and angular distributions of the solar irradiance, which are linked to the environmental conditions and the relative position of the sun to the PV module. However, majority of the energy prediction models employed absolute values of the radiation [35–38], and thus, incorporating uncertainty to their results.

The primary objective of this research study is to introduce a spectral correction regards to the wavelength dependence into the photocurrent generation prediction models applicable to bifacial PV modules integrated into APV systems. Conventionally, these models have relied upon absolute values of irradiance and albedo, often neglecting the temporal evolution of crops and the optical disparities between bare soil and crop zones. The outcomes of this research, coupled with the proposed methodology, stand to enhance the precision of performance predictions for PV systems incorporating bifacial PV modules. This improvement is crucial for advancing the accuracy of business models essential for widespread adoption of this PV technology. In pursuit of this objective, our methodology incorporates spectral measurements of irradiance, encompassing Global Horizontal Irradiance (GHI), Direct Normal Irradiance (DNI), and Diffuse Horizontal Irradiance (DHI). Moreover, the methodology proposed integrates the spectral reflectivity of both soil and vegetation, with these values derived from experimental data monitored over a period of time to test the influence of the crop growth. This information presents an additional novel perspective by examining the dynamic optical properties resulting from the natural evolution of crops over time and elucidates how these parameters impact the photocurrent on the rear side of bifacial PV modules. Two experimentally distinct sky conditions, namely a clear and a hazy sky condition characterized by elevated diffuse irradiance, are considered to conduct a sensitivity test of the proposed methodology.

A key element of the methodology involves the incorporation of the view factor procedure as function of the sun height to consider the effect of inter-row distance, tracker height, shadows and crop surface. By leveraging this approach, we compare the photocurrent predictions derived from spectral values under various boundary conditions. These results are subsequently juxtaposed against predictions expected when relying on absolute values, as in common in the majority of commercial software applications. Through this comparative analysis, we aim to underscore the efficacy of our proposed spectral correction in enhancing the accuracy of photocurrent predictions for bifacial PV modules in diverse environmental conditions. The overarching goal is to contribute valuable insights that will foster advancements in the adoption and optimization of bifacial PV technology within the broader context of renewable energy systems.

While previous studies have examined aspects such as view factor theory and spectral irradiance data separately, our research fills a significant gap by integrating these parameters into a novel unified model to predict the photocurrent of APV systems. The proposed model is a theoretical exploration based in experimental measurements, including solar irradiance (absolute and spectral data), and optical reflectance of soil and crops. Importantly, we incorporate dynamic spectral properties of crops throughout their natural growth cycle, a feature not addressed in prior literature. In this study, we predict the photocurrent of bifacial PV modules by synthesizing various information sources previously reported, including the view factor model for crucial PV plant design considerations (such as inter-row distance, shadows, and tracker height), spectral and absolute irradiance data, spectral reflectivity of crops and ground, and the dynamic evolution of crop optical properties.

2. Materials and methods

The methodology steps to predict the bifacial photocurrent gain in

APV systems are succinctly outlined in Fig. 3.

The initial stage of the process involves the optical characterization of the ground to ascertain the spectral reflectivity $R(\lambda)$. It is defined as the ratio of the upward hemispheric ground-reflected irradiance $GHI_R(\lambda)$, to the sky Global Horizontal Irradiance $GHI(\lambda)$, for each wavelength (λ), which can be represented as follows [39]:

$$R(\lambda) = \frac{GHI_R(\lambda)}{GHI(\lambda)} \tag{1}$$

Traditionally, it is also defined as an absolute reflectivity that is non-wavelength dependent, calculated as the quotient of the integer result [39]:

$$R = \frac{\int_{\lambda_i}^{\lambda_f} GHI_R(\lambda)d\lambda}{\int_{\lambda_i}^{\lambda_f} GHI(\lambda)d\lambda} \tag{2}$$

However, in this research case, Eq. (1) will be employed to account for the spectral influence of the ground and the dynamic effects of the crop growth cycle on bifacial PV performance. Considering absolute and constant reflectivity values for the ground and crop induces significant deviations in the photocurrent prediction for APV systems. Spectral changes in the crop area and bare soil were measured throughout a growing season under varying precipitation and irradiance regimes, resulting in different soil conditions and moisture content. The equipment used for this measurement is a dual detector spectrometer (Unispec-DC, PP System, Amesbury, MA, USA) that measures solar irradiance and target reflectance simultaneously. The spectrometer measures irradiance in 256 contiguous bands for both upwelling and downwelling radiation covering a nominal spectral range from approx. 310 nm to 1100 nm. It achieves a Raileigh resolution of less than 10 nm and utilizes a diode array with a bin size of 3.3 nm. Its absolute accuracy is less than 0.3 nm, ensuring reliable measurements. Synchronization accuracy is approximately 20 μs, and scan time is typically under 1 s, excluding integration time, which can be adjusted from 3 to 3200 ms to accommodate different measurement requirements. The down-facing detector is a fiber optic fitted with a field of view (FOV) restrictor of 20°, and the upward looking sensor head is fitted with a cosine diffuser. Fiber optic inputs are equipped with standard SMA 905 connectors for easy compatibility. Throughout an entire crop cultivation cycle, spectral reflectance measurements were taken using the Unispec-DC spectrometer, which allowed to characterize and analyze the reflectance spectrum dynamics of the crop at various growth stages. The same instrumentation and methodology were used to determine the effect of tillage and varying moisture conditions on the bare soil spectral reflectance. The crop reflectance data corresponds to that of a cereal crop (rice) grown under aerobic conditions, so it can be a good representative of other cereal specifies frequently exploited in APV systems.

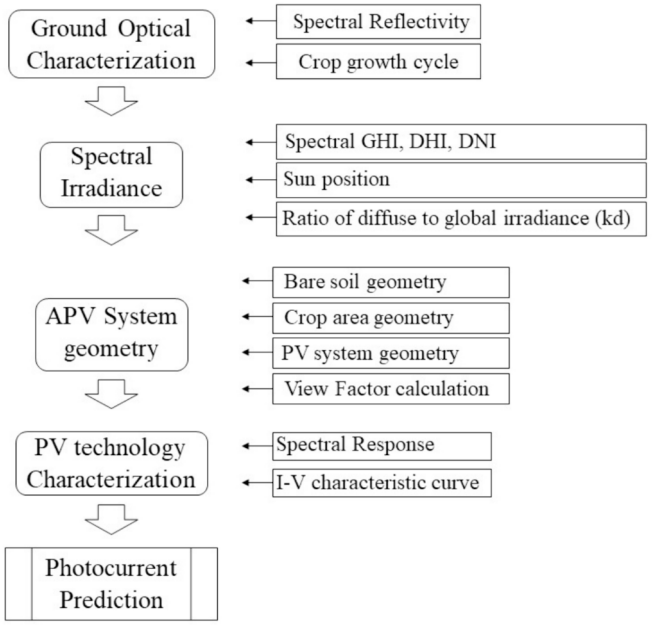

Fig. 3. Procedure to evaluate the bifacial photocurrent gain in APV systems. Phases are identified on the left, and detailed input for each phase are described on the right.

The second phase consists of the characterization of the total and spectral irradiance. The total DHI, DNI and GHI irradiance has been measured using first class calibrated Kipp and Zonen radiometers. The CMP21 model is utilized for measuring the GHI component, while the CMP10 and CHP1 models are employed for measuring the DHI and DNI, respectively. All equipment is calibrated according to ISO 9060:1990 standards, with a spectral range of 285 to 2800 nm, sensitivity ranging from 7 to 14 $\mu V/W/m^2$, and spectral selectivity of less than 3 %. Instantaneous spectral irradiance has been measured through a factory calibrated EKO MS-711N spectroradiometer. The equipment was configured with collimating tubes to narrow the field of view of the spectroradiometers aperture to 5°. Exposure time ranged from 10 ms to 5 s, depending on the intensity of the irradiance conditions. One of the spectroradiometers was integrated into a tracker (with an accuracy of $<0.01°$) to automatically follow the sun (DNI), while measurements of GHI and DHI were taken horizontally and coupled to a rotation shadow band unit (RSB-01). As the RSB rotates, four measurements are acquired: in the first position, the shadow band rests outside of the instrument field of view; in the second position, the shadow band stops at -5^{circ} from the sun disk; in the third position, the RSB covers the solar disk to perform the measurement; and in the fourth position, the shadow band stops $+\ 5^{\text{circ}}$ after the sun disk. Record spectral data every minute in steps of 0.5 nm, covering a bandwidth from 300 to 1100 nm, with a bandpass nominally < 7 nm (defined as the full width at half maximum (FWHM)), and a wavelength accuracy of $+/-$ 0.2 nm [40]. Additionally, this equipment was used in conjunction with a data logger (Campbell Scientific CR1000) to record the required parameters. The devices are installed at the University of Seville (Spain: 37.41 N, 6.01 W). The measurements were taken at the mentioned location; however, the methodology is applicable to any location where spectral irradiance data are available.

The third phase is crucial for determining the irradiance on the rear side of the bifacial PV module. The irradiance on the front side of the bifacial PV module (G^{front}) can be calculated by [41]:

$$G^{front} = G_b R_b + G_{d,tilt} + R\hat{A}{\cdot}GHI\left(\frac{1-cos\beta}{2}\right) \tag{3}$$

where G_b represents the beam irradiance on a horizontal surface; R_b is the ratio of the beam irradiance on the tilted surface to that on a horizontal surface; $G_{d,tilt}$ is the total tilted diffuse irradiance, and the most extended procedure to evaluate this parameter is the model of Pérez [42]; R is the reflectivity coefficient; and β is the PV module tilt angle. For this research case it is considered that the PV module is mounted on one axis-tracker, which is the most representative situation for large-scale PV systems, so β match with the sun height.

The irradiance on the rear side of the bifacial PV module (G^{rear}) is calculated following the Appelbaum model [34] and the view factor theory, assuming that the row of PV modules in any array is infinitely long due to its length being significantly greater than the distance between adjacent arrays. In any energy transfer process, the view factor is defined as the portion of the radiative heat flux leaving surface A that strikes surface B. That is, the view factor measures how effectively one surface can see another surface, solely from a geometric perspective. View factors play a crucial role in transferring irradiances from horizontal planes to tilted planes and in considering potential losses associated with shadows or different surface material properties. It is also

assumed a Lambertian diffuse reflection anisotropic distribution instead of a specular pattern.

$$G^{rear} = GHI\hat{A}\cdot\left[R_g\left(F_{u,g}^{rear}+F_{s,g}^{rear}\right)+R_c\left(F_{u,c}^{rear}+F_{s,c}^{rear}\right)\right]+DHI\left(\frac{1+cos\beta}{2}\right) \tag{4}$$

where *GHI* and *DHI* denote the global and diffuse horizontal irradiance spectra, respectively; R_g and R_c represent the ground and crop reflectivity coefficients, respectively. The term F_i^j accounts for various view factor coefficients, where the subscripts u,s,g,c denote "unshadow", "shadow", "ground" and "crop", respectively. The calculation of these view factors employs Hottel's crossed-string rule [34] as depicted in Fig. 4. As an illustrative example, Eq. (3) outlines the procedure for calculating the view factor of the shadow effect on the bare soil surface [43]:

$$F_{s,g} = \frac{\sum crossed\ \ strings - \sum uncrossed\ \ strings}{2\hat{A}\cdot source\ \ string} = \frac{AD+BE-AE-BD}{2\hat{A}\cdot AB} \tag{5}$$

Additionally, the angular losses factors of the direct (f_{DNI}), diffuse (f_{DHI}) and reflected (f_r) irradiance can be obtained through the following equations [13]:

$$f_{DNI} = \frac{exp\left(-cos\left(\frac{\beta}{a_r}\right)\right)-exp\left(\frac{-1}{a_r}\right)}{1-exp\left(\frac{-1}{a_r}\right)} \tag{6}$$

$$f_{DHI} = exp\left[\frac{-1}{a_r}\left(c_1\left(sin\beta+\frac{\pi-\beta-sin\beta}{1+cos\beta}\right)+c_2\left(sin\beta+\frac{\pi-\beta-sin\beta}{1+cos\beta}\right)^2\right)\right] \tag{7}$$

$$f_r = exp\left[\frac{-1}{a_r}\left(c_1\left(sin\beta+\frac{\beta-sin\beta}{1-cos\beta}\right)+c_2\left(sin\beta+\frac{\beta-sin\beta}{1-cos\beta}\right)^2\right)\right] \tag{8}$$

where a_r is the specific angular loss coefficient for each PV technology (typically 0.17 for crystalline solar cells), and the values of other parameters can be found in the reference [44].

The coordinates of the various points in Fig. 4 are incorporated into a Matlab code to develop a comprehensive APV simulator. This simulator enables the calculation of the irradiance on the rear surface of the bifacial PV module as a function of factors such as the distance to the bare soil or crop ground, albedo coefficients of bare soil or crops, incident angle, tracker height, the number of PV modules installed in the tracker, and other relevant parameters.

The final stage of the modeling process involves incorporating the irradiance output from phase 3 into the bifacial PV module to assess the ratio between the current density generated on the rear side and the front side. This ratio, as per the described procedure, is directly influenced by the reflection factors previously discussed. Various bifacial PV modules are currently available in the market, each exhibiting distinctive characteristics. These include the PERT topology known for its lower susceptibility to light-induced degradation, PERL topology with boron locally diffused in the contact regions on the rear side, PERC widely utilized in large-scale PV systems, IBC type without a metal grid contact on the front side, and HIT, distinguished by its n-type. For this research study, a PERC bifacial PV module from JA Solar, extensively employed in contemporary large-scale PV systems, is selected. The technical specifications are comprehensively outlined in Table 1.

To assess the sensitivity of the bifacial PV module to ground-reflected irradiance, this research employs external quantum efficiency (EQE) data to evaluate the performance of the device. The EQE quantifies the efficiency of converting incident photons to electrons within the solar cell, making it a wavelength-dependent function. The examination of the EQE plot enables the interpretation of spectral regions contributing

Table 1
Bifacial PV module datasheet.

Dimensions [cm^2]	21,900
No. of cells	156 (6x26)
Maximum Power (P_{max}) [W]	450
Open Circuit Voltage (V_{oc}) [V]	53.58
Maximum Power Voltage (V_{mp}) [V]	45.28
Short Circuit Current (I_{sc}) [A]	10.46
Maximum Power Current (I_{mp}) [A]	9.94
Module efficiency (η) [%]	20.4

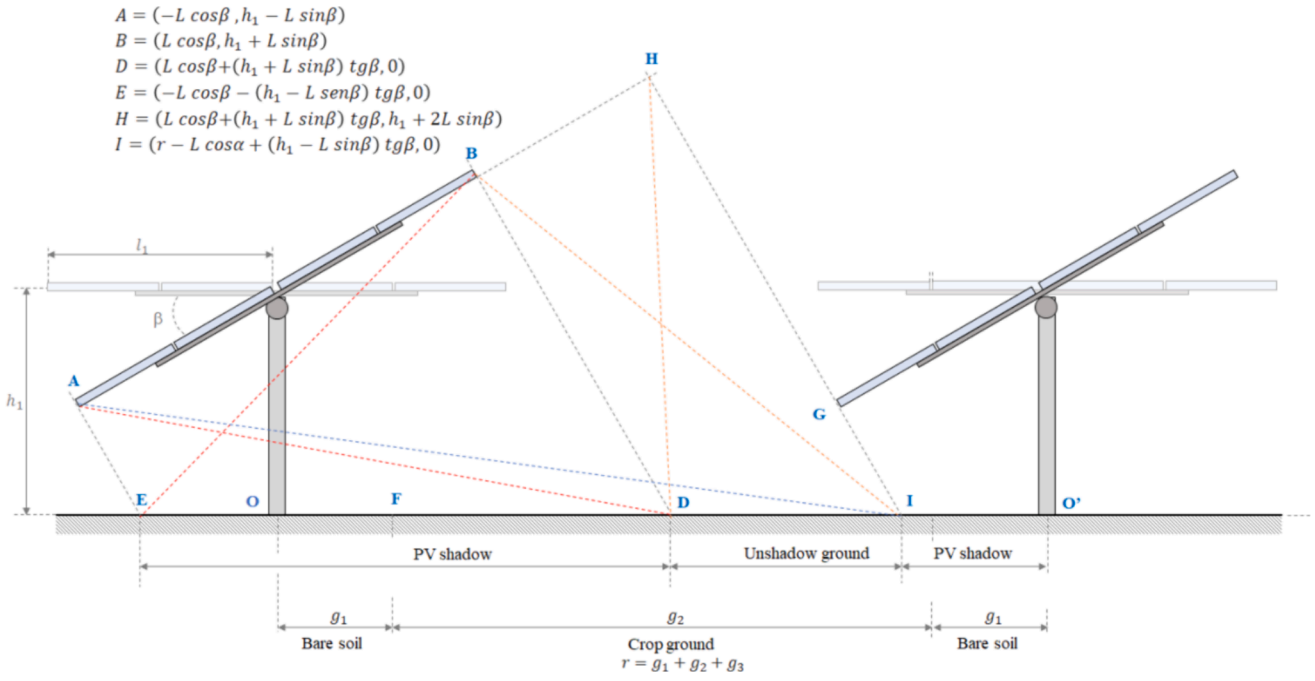

Fig. 4. APV system geometry to calculate view factor coefficients in two surfaces of infinite lengths, upon the surface is shadow/unshadow and bare soil/crop.

to photocurrent generation. Furthermore, EQE facilitates the computation of short-current density (J_{sc}) for the device [45]:

$$J_{sc} = \int_{\lambda_1}^{\lambda_2} EQE(\lambda)\hat{A}\cdot G(\lambda)d\lambda \quad (9)$$

where $G(\lambda)$ represents the incident irradiance on the PV module. A detailed analysis of the EQE offers insights into optical losses concerning a reference condition. Consequently, for accurate photocurrent prediction in APV systems, where irradiance is influenced by the spectral performance of various components, this calculation is paramount to obtain precise results in terms of photovoltaic energy generation.

3. Results and discussion

In this section, our approach is centered on elucidating the key components essential for constructing the energy model, as delineated in the preceding sections. Each of these components will undergo a comprehensive analysis to unveil the individual nuances and contributions. Subsequently, a meticulous compilation of these analyzed components will be undertaken to generate a comprehensive report on the final photocurrent generated by the APV system. A critical aspect of this analysis involves a dedicated exploration into the sensitivity of each component.

3.1. Ground optical characteristics

The temporal evolution of the disparity in diurnal crop spectral reflectivity is illustrated in Fig. 5, showcasing examples over dry and wet soil conditions. The composition of the soil, the percentage of surface covered by the crop, and the type of crop, has a high influence on the albedo. Assuming a uniform azimuthal orientation distribution and a random spatial arrangement of leaf elements [46], the inclination distribution function undergoes modifications throughout the crop growth cycle, influencing the interception of irradiance. Consequently, the percentage of soil impacting ground reflectance diminishes over time.

Additionally, the spectral reflectivity of most green leaves exhibits similarity, explicable through the selective absorption of irradiance by leaf pigments and water. Notably, leaf pigments such as carotenoids and chlorophyll exhibit pronounced absorption in the visible region, with a peak absorption range around 400–650 nm. Beyond this spectral range, neither leaf pigments nor water significantly interact with irradiance, resulting in elevated reflectivity. Generally, a crop's spectral reflectivity is primarily dictated by the probability of photon interaction with either the crop or the soil surface. Nevertheless, physiological processes within crops introduce variations in leaf optical properties, thereby offering an avenue to assess crop health diagnosis through optical characterization [47,48].

As depicted in Fig. 5, leaf spectral reflectivity experiences an augmentation in the Near-Infrared (NIR) range due to the influence that canopy architecture, vegetation density, and other factors related to leaf structure and canopy arrangement plays on NIR reflectivity. Statistical comparisons were executed through one-way ANOVA test at 95 % confidence level ($p < 0.05$). The maximum reflectivity values are observed to be 47 % at 779 nm for the early growth stage and achieving a maximum value of 57 % for the same wavelength. Moreover, it is also observed how the change of bare soil by crops reduces the spectral reflectivity of the ground from 25 % to 10 % in the range of 550 to 700 nm. This observation clearly has a significant influence on the spectral irradiance incoming on the rear side of the bifacial PV module, reducing its energy generated. The crop reflectivity data corresponds to that of a cereal crop (rice) grown under aerobic conditions, so it can be a good representative of other cereal specifies frequently exploited in APV systems.

The significance of comprehending reflectivity for accurate photocurrent predictions in bifacial PV modules is observed in Fig. 5. This optical parameter is inherently influenced by the morphological characteristics of the considered surface, imparting either an isotropic or anisotropic albedo environment. Notably, existing literature and widely adopted PV design software often assume the ground to behave as a Lambertian reflector, characterized by uniform reflection in all directions. However, under these conditions, the spectral reflectivity of the ground remains invariant throughout the day, leading to an overestimation of predicted photocurrent. For instance, the spectral reflectivity of compact soil exhibits increased specularity when the soil is compacted compared to its tilled state before crop plantation, consequently favoring a more diffuse reflectivity pattern. Additionally, when the soil is irrigated, the reflectivity is also reduced due to the water absorption. In light of these considerations, various optical models are available in the literature [49] (Table 2), and their incorporation into the modelling process is imperative to assess the sensitivity of predicted photocurrent to ground morphology conditions. This approach acknowledges the dynamic nature of ground reflectivity and aims to refine accurate photocurrent predictions by accounting for realistic surface characteristics.

Table 3 summarizes the results of the absolute reflectivity obtained for each spectrum showed in Fig. 5, as per Eq. (2). These values will also

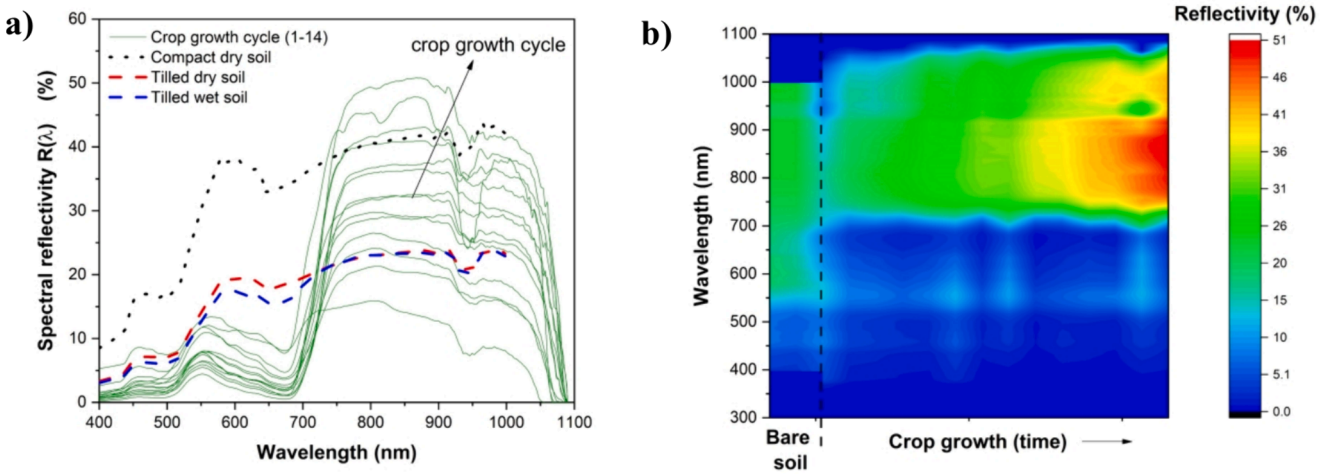

Fig. 5. Spectral reflectivity measured as function of wavelength (a) and dynamic crop growth (b), both compared to different types of soil: tilled dry (red dash line), tilled wet (blue dash line) and dry compact (black dot line). (For interpretation of the references to colour in this figure legend, the reader is referred to the web version of this article.)

Table 2
Optical models for the ground reflectivity.

Isotropic models	
Liu-Jordan	$R_{dif} = \frac{1+cos\beta}{2}$
Korokanis	$R_{dif} = \frac{1}{3}(2+cos\beta)$
Badescu	$R_{dif} = \frac{1}{4}(3+\cos(2\beta))$
Anisotropic models	
Willmot	$R_{dif} = \frac{B_N r_b}{S_0} + C_\beta\left(1-\frac{B_N}{S_0}\right)$
Gueymard	$R_{dif} = (1-N_g)R_{d0} + N_g R_{d1}$
Ma-Iqbal	$R_{dif} = k_t r_b + (1-k_t)\left(\frac{1+cos\beta}{2}\right)$

be considered in the model to highlight differences in photocurrent prediction when absolute or spectral values are utilized as raw data.

3.2. Solar irradiance characteristics

The energetic impact of the spectral irradiance is of particular importance to determine the photocurrent estimation of any PV system, but fundamental for APV systems based on bifacial PV modules. However, spectral irradiance database is not readily available at any location with sufficient temporal and spatial resolution [50], so typically researchers use irradiance absolute values, but its uncertainty is propagated directly to the photocurrent prediction. We have selected two days visually identified as "clear sky" and "hazy sky" by experienced experts. The selected clear and hazy sky days correspond to the days 22nd July and 28th June 2023, respectively. Both days were monitored at high resolution, getting data at each nanometer with a 1-min frequency. Both set of datasets are used to investigate the sensitivity of the methodology proposed for evaluate the photocurrent generated by the APV system. The daily radiation profiles of the absolute GHI, DNI and DHI components are shown in Fig. 6.

Fig. 7 shows the different components of the spectral irradiance measured under two different conditions: clear and hazy sky. Fig. 7 illustrates that when solar radiation reaches the Earth's surface, it not only impacts irradiance but also influences spectral components. The solar irradiance spectrum exhibits variability throughout the day, a phenomenon evident in all components: GHI, DNI, and DHI. The DHI component is conventionally understood to be uniformly distributed across the sky under clear sky, with the highest values expected during midday (Fig. 7c), corresponding to the typical orientation of PV modules in one-axis tracker. However, Fig. 7f demonstrates how the DHI spectral distribution undergoes modification on a typical day characterized by hazy sky conditions, where an increase in atmospheric mass results in broader spectrum with heightened intensity. The diffuse fraction correlation (k_d) is subsequently computed to assess the impact of the spectral diffuse irradiance component on the selected days for this analysis (Fig. 8) [51].

$$k_d(\lambda) = \frac{DHI(\lambda)}{GHI(\lambda)} \tag{10}$$

While the selected clear sky conditions yield diffuse fraction coefficient (k_d) values closer to 0, the day with hazy sky conditions presents higher values, particularly during sunset and noon hour. Moreover, on the hazy sky day, k_d exhibits notable inhomogeneity in terms of wavelength dependence, underscoring the significance of incorporating spectral irradiance data for accurate energy yield predictions. In the subsequent section, this information is juxtaposed with the spectral sensitivity of the PV module.

Table 4 compiles the absolute values of solar irradiance components measured on the same days using a conventional pyranometer instead of one spectroradiometer. Although these absolute values align effectively with the integration of spectral irradiance datasets, the predicted photocurrent diverges in both cases due to the wavelength dependent nature of the quantum efficiency of the solar cell.

Taking into account the spectral solar irradiance and the spectral reflectivity of the ground and acknowledging the dependence of this parameter on the extent of crop coverage over the soil, the distribution of irradiance incident on the rear side of the bifacial PV module can be

Table 3
Absolute reflectivity R calculated from spectrum showed in Fig. 5.

Bare soil													
Compact						Tilled dry							Tilled wet
27 %						14 %							13 %
Crop growth cycle													
1	**2**	**3**	**4**	**5**	**6**	**7**	**8**	**9**	**10**	**11**	**12**	**13**	**14**
10%	9%	9%	10%	12%	13%	12%	14%	12%	14%	15%	16%	19%	18%

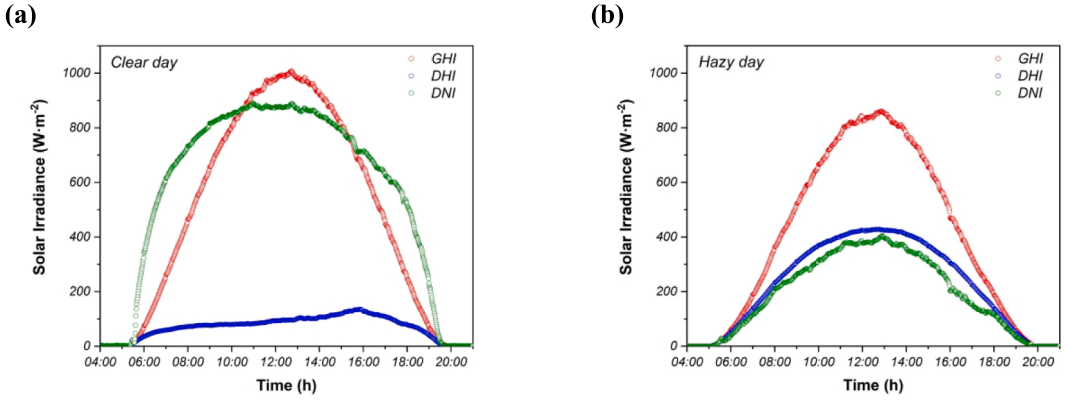

Fig. 6. Daily absolute GHI, DNI and DHI values monitored for two different days: clear sky (a) and hazy day (b).

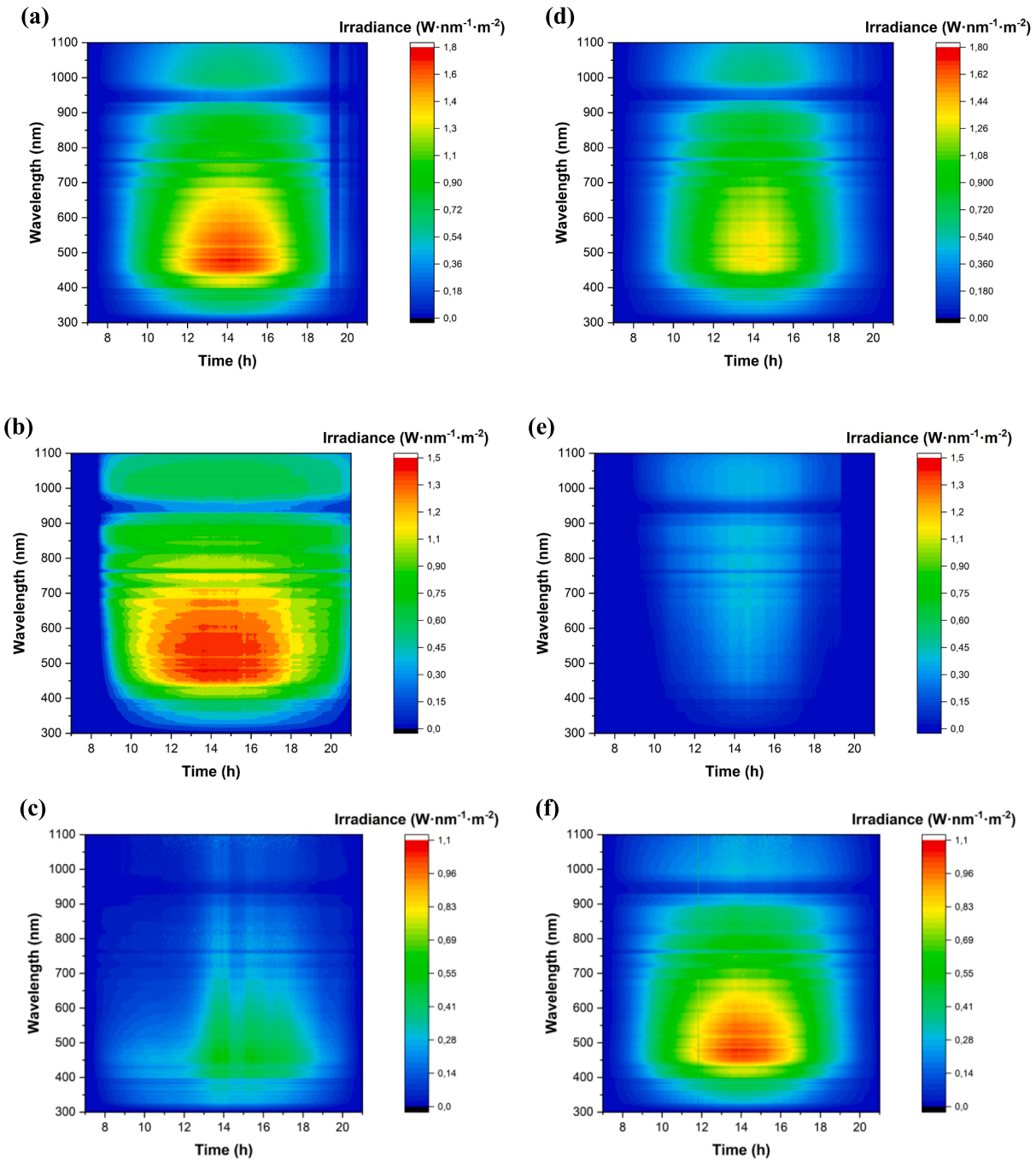

Fig. 7. Spectral solar irradiance measured for two different days, sunny conditions a) GHI, b) DNI, c) DHI; and haze conditions d) GHI, e) DNI, f) DHI.

simulated (Fig. 9). This calculation is performed with the experimental data recorded with the tracker positioned at 45°, corresponding to 11 h GMT on July 22nd. The calculated irradiance exhibits a nonuniformity of 27 % for the lower PV module and 8 % for the highest PV module installed in the tracker in a 2 V configuration. It is shown that the distribution is not uniform with the lower side of the PV module receiving higher irradiance, which is explained by the isotropic distribution of DHI component and the consideration of shadowing effects through the corresponding view factors.

Furthermore, it is observed that solar irradiance intensity increases when the ground is fully covered by crops, and no bare soil is considered. This phenomenon occurs because, despite the spectral reflectivity of bare soil displaying more uniform values than crops, the latter exhibit higher reflectance in the range of 600 to 1100 nm. These results are aligned with previous research reported by Monokroussos et al. [52] who performed a similar approach but considering only grave ground albedo conditions without any influence from the crop for APV applications. This inhomogeneities are negligible if the modeling is carried out using absolute solar irradiance and ground reflectivity values.

3.3. PV module spectral influence

Based on the semiconductor materials chosen for the manufacturing of the solar cell, and their respective band gaps, significant variations in the sensitivity of diverse PV technologies to spectral solar irradiance can be discerned. Fig. 10 [53] shows the spectral response of various PV technologies available at large scale in the commercial market, all of which have purportedly been engineered with bifacial properties

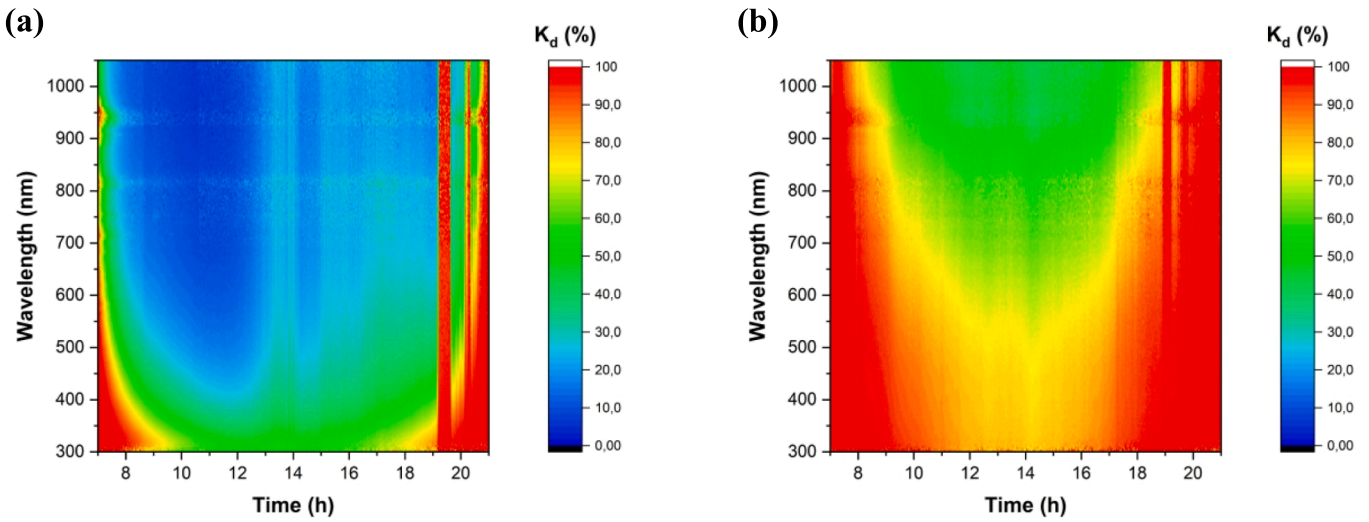

Fig. 8. Diffuse fraction coefficient (k_d) calculated for a) clear sky, and b) hazy sky.

Table 4
Absolute daily irradiance measured for both selected days: a) clear sky, and b) hazy sky conditions.

	Clear sky	Hazy sky
GHI (kWh·m^{-2}·day^{-1})	8.29	6.73
DNI (kWh·m^{-2}·day^{-1})	9.62	3.25
DHI (kWh·m^{-2}·day^{-1})	1.18	3.84

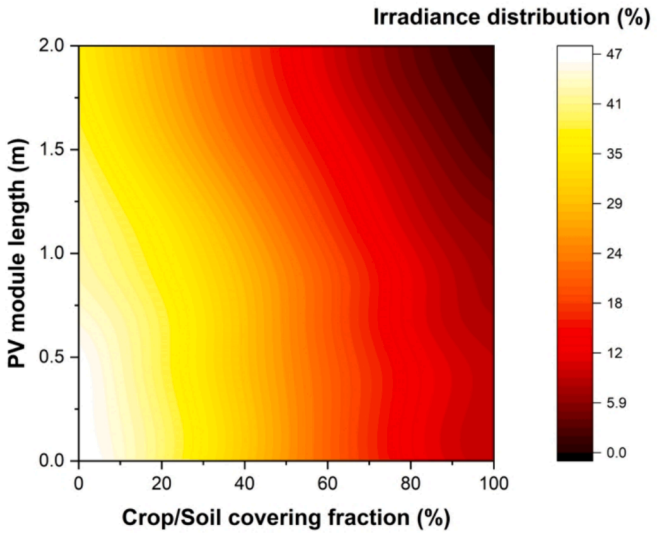

Fig. 9. Solar irradiance relative distribution simulated on the rear surface of the bifacial PV, as a function of the crop cover fraction versus soil

[54–56]. A comparison between Fig. 10 and Fig. 5 distinctly reveals that a-Si and CdTe technologies exhibit low photocurrent generation in any bifacial APV system. This is attributed to the mismatch in spectral sensitivity concerning wavelength with the reflected irradiance. Nonetheless, when the prediction of photocurrent is calculated according to Eq. [11], utilizing absolute values of ground reflectivity (ρ), absolute irradiance (G_{rear}), and the IV typical optoelectronic parameters (J_{sc}, V_{oc}, FF) derived from each PV technology, there exists no criterium to dismiss a-Si and CdTe PV technologies for bifacial APV applications. The inclusion of spectral data in the model is imperative to ensure the accurate photocurrent predictions [57].

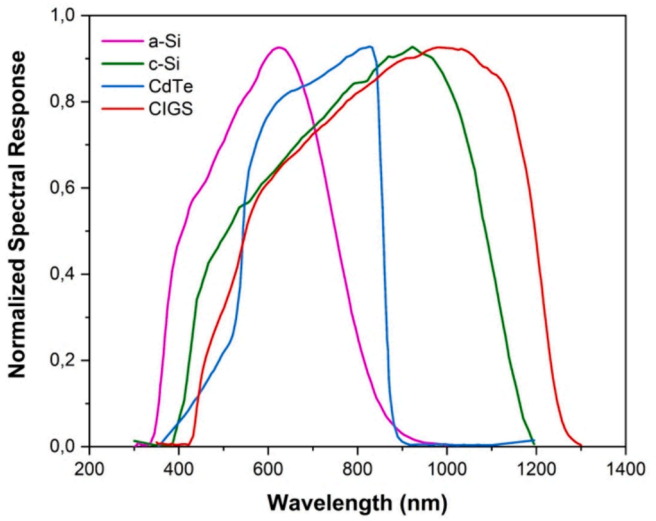

Fig. 10. Normalized spectral response for commercial large-scale PV technologies [34].

$$P_{out} = \frac{J_{sc}\hat{A}\cdot V_{oc}\hat{A}\cdot FF}{G_{rear}} \tag{11}$$

Additionally, Riedel-Lyngskaer et al. [16] reported the spectral response of different bifacial PV samples based on c-Si (IBC, PERT and PERC), noting negligible distinctions among them and between front and rear sides of the PV module.

To assess the feasibility of bifacial PV modules in one-axis tracking for APV applications, we have adapted the methodology outlined by Mouhib et al. [4] to determine the generated front and rear photocurrents, along the photocurrent ratio (ξ) [Eqs. (12)–(14)]:

$$J_{sc}^{front} = \frac{\int SR_{front}(\lambda)\hat{A}\cdot G_{front}(\lambda)d\lambda}{\int G_{front}(\lambda)d\lambda} \tag{12}$$

$$J_{sc}^{rear} = \frac{\int SR_{rear}(\lambda)\hat{A}\cdot G_{rear}(\lambda)d\lambda}{\int G_{rear}(\lambda)d\lambda} \tag{13}$$

$$\xi = \frac{J_{sc}^{rear}}{J_{sc}^{front}} \tag{14}$$

The integral limits encompass the wavelength range corresponding to the spectral response of the solar cell and the irradiance measurement range. Under this definition, if the bifacial PV module receives equivalent energy on both faces, the photocurrent ratio (ξ) attains a value of 1. This metric proves valuable for quantifying the photocurrent enhancement on the rear side of the PV device, contingent upon the geometrical characteristics of the APV system and the optical properties of the ground. Another pertinent advantage of the photocurrent ratio (ξ) lies in assessing variations in the spectral conditions of solar irradiance. In cases where the absolute energy incident on both sides of the bifacial PV module remains the same but experiences spectral modifications due to ground reflectance, the photocurrent ratio (ξ) deviates from 1. These nuances cannot be captured using conventional Eq. (11) and absolute values to predict the photocurrent.

Fig. 11 and Table 5 illustrate the photocurrent generated by the rear side of the bifacial PV module under various sky conditions as function of the ground reflectance. The aim is to emphasize the significance of incorporating spectral raw data in photocurrent predictions. It is observed that, under clear sky conditions where the direct normal irradiance (DNI) is predominant (Fig. 7b), the maximum photocurrent occurs when the tracker is nearly horizontal, corresponding to midday. In contrast, under hazy sky conditions where the diffuse horizontal irradiance (DHI) is dominant (Fig. 7e), the maximum photocurrent is achieved when the tracker is in quasi-vertical position to maximize the Lambert coefficient, which is dependent on the cosine of the tracker inclination.

Table 5
Comparison of estimated front and rear side bifacial PV module photocurrent ratio (ξ) under different sky conditions and ground reflectance when using spectral or absolute raw data as input.

Crop/bare soil ratio (%)	Clear sky conditions		Hazy sky conditions	
	ξ spectral data	ξ absolute data	ξ spectral data	ξ absolute data
0	0.111	0.165	0.143	0.165
27	0.103	0.164	0.136	0.164
53	0.086	0.163	0.118	0.163
80	0.083	0.161	0.114	0.161
100	0.081	0.160	0.112	0.160

Furthermore, ground conditions exert a substantial influence on the rear side photocurrent. As ground increases the crop/bare soil ratio, the reflectance rises in those wavelengths matching well with the solar cell spectral response, thereby enhancing the photocurrent generated on the rear side of the bifacial PV module. This observation underscores the advantages of hybrid conventional PV systems with agricultural applications, leveraging crop reflectivity in the bifacial PV module.

Analysis of Fig. 11, specifically parts c) and d), leads to the conclusion that the influence of ground optical properties becomes more pronounced when the tracker angle increases, owing to the view factor in such configuration. While, under clear sky conditions, the difference between front and rear photocurrent remains relatively constant throughout the day, it is notable that under hazy sky conditions, the

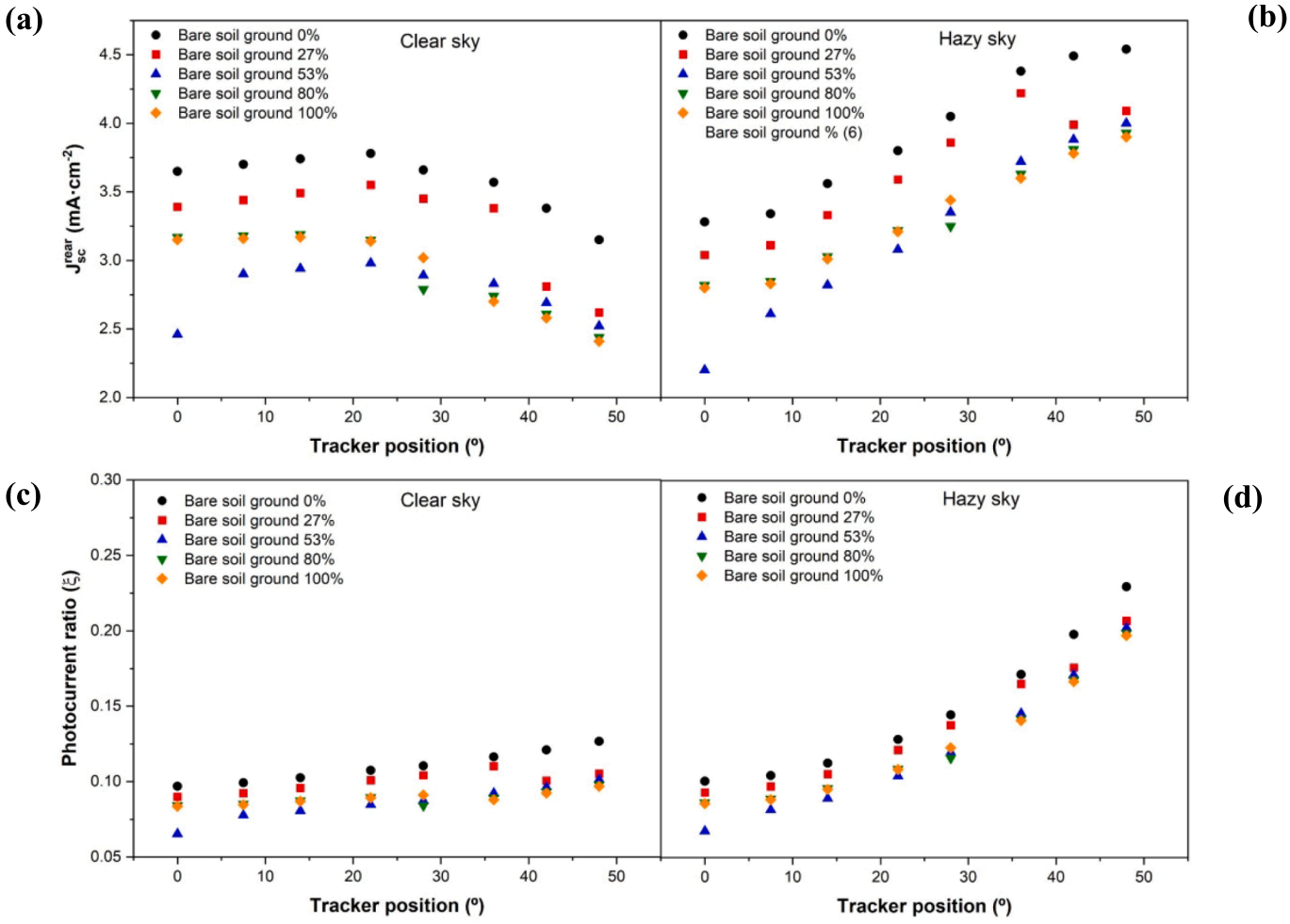

Fig. 11. Photocurrent generated in the rear side of the bifacial PV module as function of the shaded, bare soil and crop surface using spectral irradiance data for a clear sky (a) and hazy sky conditions (b). Rear and front photocurrent ratio (ξ) generated in clear sky (c) and hazy sky (d) conditions.

ratio (ξ) varies from 0.09 to 0.27 over the day. Such variation and its influence in the photocurrent estimation cannot be accurately determined through absolute values of ground reflectance and solar irradiance.

Table 6 contrasts the photocurrent ratio (ξ) estimation of the bifacial PV module under different ground and sky conditions, utilizing both spectral and absolute values. Relative difference percentage (ΔJ) between absolute and spectral photocurrent is defined as:

$$\Delta J(\%) = \frac{J_{sc}^{(abs)} - J_{sc}^{(spec)}}{J_{sc}^{(spec)}} \times 100 \quad (15)$$

For this calculation, the tracker is considered to be in an intermediate position (30°), which corresponds to 12 h GMT conditions during the measurement campaign, irradiance is 990 W·m^{-2} for clear sky and 843 W·m^{-2} for hazy sky, soil average reflectance is 33 %, and crop average reflectance is 16 %.

The data presented in Table 6 reveals an overestimation of the rear photocurrent compared to the front in all cases when considering absolute data versus spectral data, under the specified conditions. This overestimation is consistently more pronounced under clear sky conditions, with a relative difference (ΔJ) ranging from 48.6 % to 100 %, than under hazy sky conditions, where the range is between 15.4 % and 42.9 %. As the crop/bare ratio on the terrain increases, the relative difference between both types of calculations become more prominent. Consequently, a notable relative difference (ΔJ) has been observed from the utilization of either absolute or spectral data, surpassing the intrinsic uncertainties of both measurement devices. These disparities lead to an overestimation in photocurrent when using bifacial PV modules of approximately 4.8 % to 7.9 % under clear sky conditions and 1.5 % to 2.1 % under hazy sky conditions. Furthermore, the consideration of absolute data in the calculations results in minimal sensitivity of the predicted photocurrent to changes in the level of crop coverage on the ground.

Once again, these findings underscore the recommendation of employing spectral values instead of absolute values for accurate prediction of the photocurrent in bifacial PV modules.

3.4. Photocurrent prediction analysis

Once it has been demonstrated the importance of using spectral values to predict the photocurrent in the bifacial PV module of the APV system, it is explored the sensitivity of the model to additional aspects like the natural growth of the crops and the incorporation of anisotropic optical models for the reflected irradiance in the ground. Fig. 12 illustrates the ratio (ξ) generated by the bifacial PV module during the complete growth cycle of the crop. Over this time, as consequence of the natural evolution of the leaf of the crop, the spectral reflectance changes significantly, affecting the irradiance received by the rear side of the bifacial PV module.

The ratio of photocurrent in the bifacial PV module demonstrates a pronounced dependency on the nature of input data, whether spectral or absolute. Absolute data exhibit constrained sensitivity to solar irradiance variations, regardless of atmospheric conditions (clear sky or hazy sky). In both scenarios, they consistently generate inflated photocurrent predictions compared to spectral values. Conversely, spectral data analysis reveals a distinct patter contingent on atmospheric conditions, illustrating a higher photocurrent ratio (ξ) on hazy days due to the prevailing contribution of diffuse irradiance on the rear side of the bifacial PV module.

Table 6
Comparison of relative difference between absolute and spectral photocurrent (ΔJ) under different sky conditions and ground reflectance when using spectral or absolute raw data as input.

Crop/bare soil ratio (%)	Relative difference (ΔJ(%))	
	Clear sky conditions	Hazy sky conditions
0	48.6 %	15.4 %
27	59.2 %	20.6 %
53	89.5 %	38.1 %
80	93.9 %	41.2 %
100	100.0 %	42.9 %

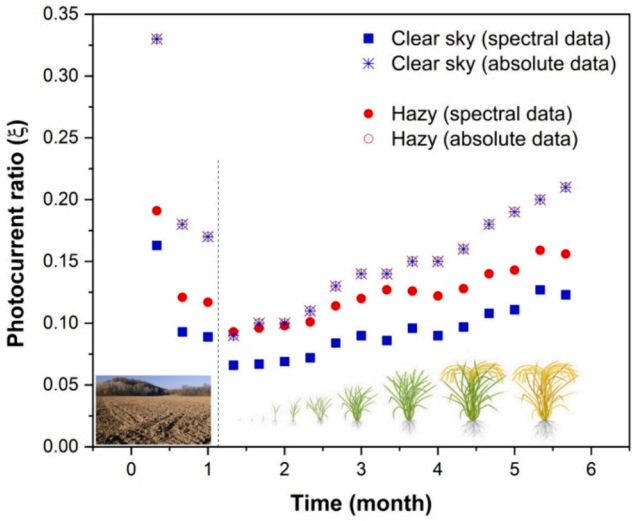

Fig. 12. Comparison of the ratio of photocurrent generated in the rear and front side of the bifacial PV module.

Significantly, ground conditions play a pivotal role, with bare and compact soil resulting in a higher short-circuit current ratio compared to surface cultivated or planted with crops. When modifying compact ground to incorporate crops into the APV system, a two-step process involving tillage and irrigation is implemented. During tillage, the reflected irradiance undergoes a transition from quasi-specular to anisotropic conditions with a directional reflection. Subsequently, during irrigation, increased humidity reduces ground reflectance, thereby minimizing reflected irradiance on the rear side of the bifacial PV module. Finally, the presence of crops modifies the reflectance model to a Lambertian reflection.

Furthermore, the growth of crops emerges as a critical factor influencing ground reflectance, leading to a noticeable enhancement of the photocurrent ratio (ξ) as plants mature. Considering ground or crop reflectivity as absolute values constant over time results in an overestimation of photocurrent in the bifacial PV module installed in the APV system. While this overestimation may be advantageous from a project's bankability perspective, it can lead to misunderstanding between the site operator and owner when the real performance ratio falls below expected values.

Given that typical crop growth cycles extend from 4 to 6 months, it becomes imperative to revisit the evolution of reflectance influence on the bifacial PV module production twice annually to ensure the accuracy of photocurrent predictions. This periodic assessment is crucial for capturing the dynamic nature of ground optical properties influenced by the growth stages of crops over an agricultural season. The reflectance dynamic evolution points out a critical factor in APV systems compared to conventional large-scale PV systems, where the ground influence in the energy production can be considered constant over time.

These findings underscore the paramount importance of incorporating spectral data for accurate photocurrent predictions in bifacial PV modules within APV systems, and subsequent energy yield estimation. The insights gained offer valuable guidance for optimizing project performance, aligning operational results with expected outcomes established during the design phase.

The dynamics of the ground influence not only the reflectance values but also the optical model, as the nature of the reflected irradiance

undergoes a transition from a cuasi-specular to a Lambertian distribution, incorporating anisotropic contributions dependent on soil characteristics and the leafiness of crops. To assess the sensitivity of the photocurrent predicted by the bifacial PV module to these models, equation [Eq. (4)] is adapted to introduce a preferential direction in the reflected light, in a similar way as explained Sun et al. [13]:

$$G^{rear} = GHI\hat{A}\cdot\left[\alpha_g\left(F_{u,g}^{rear} + F_{s,g}^{rear} + \right) + \alpha_c\left(F_{u,c}^{rear} + F_{s,c}^{rear}\right) + \left(1 - F_{anis}^{rear}\right)\left(\alpha_g + \alpha_c\right)\right] + DHI\left(\frac{1+cos\beta}{2}\right) \quad (16)$$

where the diffuse reflected irradiance is modified with the view factor F_{anis}^{rear} to emphasize a preferential orientation. The influence of considering anisotropic reflections primarily impacts the uniformity of the irradiance received on the rear side of the bifacial PV module rather than the overall photocurrent generated. Fig. 13 shows the irradiance distribution on the rear side of the bifacial PV module as function of anisotropic view factor, dependent on the geometrical pattern in the ground and the tracker height. As the tracker height increases, the influence of the anisotropic terms diminishes $\left(F_{anis}^{rear} \rightarrow 1\right)$, while for low tracker height, especially when the ground is tilled or the foliage density is low, the anisotropic terms become non-negligible.

Examining Eq. (14) elucidates that anisotropic effects manifest more prominently under clear sky conditions, where the diffuse irradiance component is lower compared to hazy sky conditions. Consequently, we infer that incorporating anisotropic terms into the model yields precise outcomes concerning the distribution of reflected solar irradiance on the rear side of the bifacial PV module. This consideration becomes particularly significant under specific boundary conditions in the APV system design: a) tilled ground; b) relatively lower tracker height; c) non-dominance of the solar diffuse irradiance component.

4. Conclusions

It has been demonstrated that employing spectral data for predicting photocurrent in APV systems provides more accurate results compared to using absolute data. The dynamic nature of soil in agrovoltaic setups introduces variability in reflectance over time, influenced by factors such as soil type (compact or tilled), crop type, and foliage level and growth cycle. Notably, the reflectivity of the soil is not constant, leading to significant deviations in energy production when integrated over time. Optimal conditions for energy production are observed when the soil is fully planted, accompanied by tall foliage that facilitates isotropic irradiance dispersion.

Spectral irradiance data collected during a clear sky day reveals that rear-side photocurrent is maximized in bifacial PV modules when the tracker position remains horizontal in APV systems. However, during hazy sky days, nearly vertical tracking proves to be more productive. Additionally, it is found that the presence of cultivated soil enhances the uniformity of irradiance on the rear side of the bifacial PV module minimizing the temperature distribution, compared to bare and tilled soil. This underscores the importance of considering the ground cover and cultivation practices when optimizing photocurrent generated in agrovoltaic systems.

In summary, our research emphasizes the importance of incorporating spectral data, accounting for ground (soil and crops) dynamics, and considering environmental conditions (sunny or hazy sky) for accurate predictions and optimization of energy output in bifacial PV modules deployed in agrovoltaic settings. Furthermore, as future research directions, we recommend for conducting additional measurements of spectral reflectance across various crops throughout their growth cycles. These measurements should be correlated with the energy production of bifacial PV modules within agrovoltaic systems, aiming to enhance the accuracy and applicability of analytical models. Additionally, we strongly recommend making spectral radiation measurements openly accessible to facilitate comparisons of PV model performance using both absolute and spectral radiation data.

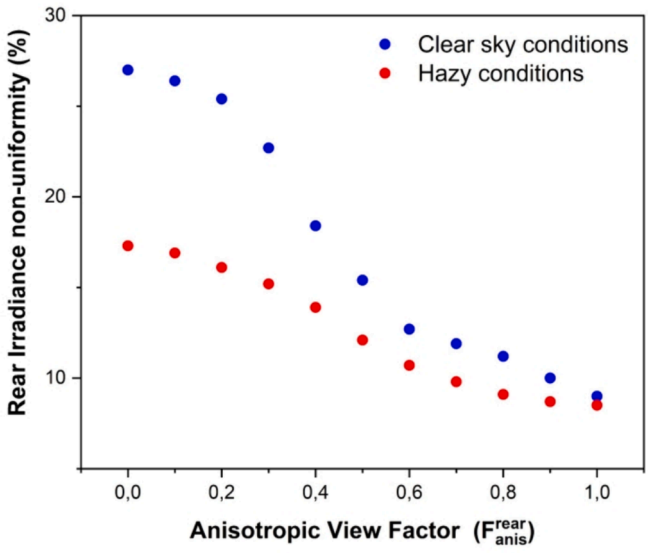

Fig. 13. Average rear irradiance non-uniformity (%) for two sky conditions, clear and hazy sky, as function of the anisotropic view factor.

Funding

This research did not receive any specific grant from funding agencies in the public, commercial, or not-for-profit sectors.

CRediT authorship contribution statement

M. Barragán Sánchez-Lanuza: Writing – original draft, Software, Methodology, Investigation, Formal analysis, Data curation. **I. Lillo-Bravo:** Writing – original draft, Resources, Methodology, Investigation, Formal analysis, Conceptualization. **G. Egea:** Writing – original draft, Resources, Formal analysis. **J.M. Delgado-Sanchez:** Writing – original draft, Supervision, Software, Resources, Methodology, Investigation, Formal analysis, Data curation, Conceptualization.

Declaration of competing interest

The authors declare that they have no known competing financial interests or personal relationships that could have appeared to influence the work reported in this paper.

Data availability

Data will be made available on request.

Acknowledgements

We would like to extend our sincere appreciation to Prof. Francisco Javier Romero Landa for fruitful contributions and insightful discussion on optics, and to Prof. Miguel Larrañeta for his support on managing the meteorological station facilities.

References

[1] Eguren J, Martínez-Moreno F, Merodio P, Lorenzo E. First bifacial PV modules early 1983. Sol Energy 2022;243:327–35.
[2] Guerrero-Lemus R, Vega R, Kim T, Kimm A, Shephard L. Bifacial solar photovoltaics – a technology review. Renew Sustain Energy Rev 2016;60:1533–49.
[3] Gu W, Ma T, Ahmed S, Zhang Y, Peng J. A comprehensive review and outlook of bifacial photovoltaic (bPV) technology. Energ Conver Manage 2020;223:113283.

[4] Mouhib E, Rodrigo PM, Micheli L, Fernández EF, Almonacid F. Quantifying the rear and front long-term spectral impact on bifacial photovoltaic modules. Sol Energy 2022;247:202–13.
[5] Al-Masri HMK, Dawaghreh OM, Magableh SK. Realistic performance evaluation and optimal energy management of a large-scale bifacial photovoltaic system. Energ Conver Manage 2023;286:117057.
[6] Juaidi A, Kobari M, Mallak A, Titi A, Abdallah R, Nassar M, Albatayneh A. A comparative simulation between monofacial and bifacial PV modules under Palestine conditions. Solar Compass 2023;8:100059.
[7] Longares JM, García-Jiménez A, García-Polanco N. Multiphysics simulation of bifacial photovoltaic modules and software comparison. Sol Energy 2023;257:155–63.
[8] Alam M, Saleem Gul M, Muneer T. Performance analysis and comparison between bifacial and monofacial solar photovoltaic at various ground albedo conditions. Renew Energy Focus 2023;44:295–316.
[9] Asgharzadeh A, Marion B, Deline C, Hansen C, Stein JS, Toor F. A sensivity study of the impact of installation parameters and system configuration on the performance of bifacial PV arrays. IEEE J Photovoltaics 2018;8(3):798–805.
[10] Ghenai C, Ahmad FF, Rejeb O, Hamid AK. Sensitivity analysis of design parameters and power gain correlations of bifacial solar PV system using response surface methodology. Sol Energy 2021;223:44–53.
[11] Jang J, Lee K. Practical performance analysis of a bifacial PV module and system. Energies 2020;13:4389.
[12] Baghel N, Manjunath K, Kumar A. Performance evaluation and optimization of albedo and tilt angle for solar photovoltaic system. Comput Electr Eng 2023;110:108849.
[13] Sun B, Lu L, Yuan Y, Oclón P. Development and validation of a concise and anistropic irradiance model for bifacial photovoltaic modules. Renew Energy 2023;209:442–52.
[14] Chantana J, Imai Y, Kawano Y, Hishikawa Y, Nishioka K, Minemoto T. Impact of average photon energy on spectral gain and loss of various-type PV technologies at different locations. Renew Energy 2020;145:1317–24.
[15] Tonita EM, Valdivia CE, Russel ACJ, Martinez-Szewcyk M, Bertoni MI, Hinzer K. Quantifying spectral albedo effects on bifacial photovoltaic module measurements and system model predictions. Progr Photovoltaic: Res Appl 2024:1–13.
[16] Riedel-Lyngskaer N, Ribaconka M, Po M, Thorseth A, Thorsteinsson S, Dam-Hansen C, et al. The effect of spectral albedo in bifacial photovoltaic performance. Sol Energy 2022;231:921–35.
[17] Monokroussos C, Gao QI, Zhang X, Lee E, Wang Y, Zou C, et al. Rear-side spectral irradiance at 1 sun and application to bifacial module power rating. Prog Photovolt Res Appl 2020;28(8):755–66.
[18] Goetzberger A, Zastrow A. On the coexistence of solar-energy conversion and plant cultivation. Int J Sol Energy 1982;1(1):55–69.
[19] Widmer J, Christ B, Grenz J, Norgrove L. Agrivoltaics, a promising new tool for electricity and food production: a systematic review. Renew Sustain Energy Rev 2024;192:114277.
[20] Grubbs EK, Gruss SM, Schull VZ, Gosney MJ, Mickelbart MV, Brouder S, et al. Optimized agrivoltaic tracking for nearly-full commodity crop and energy production. Renew Sustain Energy Rev 2024;191:114018.
[21] Dupraz C, Marrou H, Talbot G, Dufour L, Nogier A, Ferard Y. Combining solar photovoltaic panels and food crops for optimizing land use: towards new agrivoltaic schemes. Renew Energy 2011;36:2725–32.
[22] Hsu H-W, Yang C-C. Assessing land resource planning for agrivoltaics development: examining synergies approaches between government and farmers. Energy 2024;298:131363.
[23] Barron-Gafford GA, Pavao-Zuckerman MA, Minor RL, Sutter LF, Barnett-Moreno I, Blackett DT, et al. Agrivoltaics provide mutual benefits across the food-energy-water nexus in drylands. Nat Sustain 2019;2(9):848–55.
[24] Kumpanalaisatit M, Setthapun W, Sintuya H, Pattiya A, Jansri SN. Current status of agrivoltaic systems and their benefits to energy, food, environment, economy, and society. Sustain Prod Consum. 2022;33:952–63.
[25] Prakash V, Lunagaria MM, Trivedi AP, Upadhyaya A, Kumar R, Das A, et al. Shading and PAR under different density agrivoltaics systems, their simulation and effect on wheat productivity. Eur J Agron 2023;149:126922.
[26] Tahir Z, Zafar Butt N. Implications of spatial-temporal shading in agrivoltaics under fixed tilt & tracking bifacial photovoltaic panels. Renew Energy 2022;190:167–76.
[27] Ma Lu S, Yang D, Anderson MC, Zainali S, Stridh B, Avelin A, et al. Photosynthetically active radiation separation model for high-latitude regions in agrivoltaics systems modeling. J Renew Sustain Energy 2024;16:013503.
[28] Sojib Ahmed M, Rezwan Khan M, Haque A, Ryyan Khan M. Agrivoltaics analysis in a techno-economic framework: understanding why agrivoltaics on rice will always be profitable. Appl Energy 2022;323:119560.
[29] Waghmare R, Jilte R, Joshi S, Tete P. Review on agrophotovoltaic systems with a premise on thermal management of photovoltaic modules therein. Sustain Res Energy Environ 2023;30:25591–612.
[30] Sun X, Khan MR, Deline C, Alam MA. Optimization and performance of bifacial solar modules: a global perspective. Appl Energy 2018;212:1601–10.
[31] Khan MR, Hanna A, Sun X, Alam MA. Vertical bifacial solar farms: physics, design, and global optimization. Appl Energy 2017;206:240–8.
[32] Mouhib E, Fernández-Salas A, Pérez-Higueras PJ, Fernández-Ocaña AM, Micheli L, Almonacid F, et al. Enhancing land use: integrating bifacial PV and olive tress in agrivoltaics systems. Appl Energy 2024;359:122660.
[33] Ledesma JR, Almeida RH, Martinez-Moreno F, Rossa C, Martín-Rueda J, Narvarte L, et al. A simulation model of the irradiation and energy yield of large bifacial photovoltaic plants. Sol Energy 2020;206:522–38.
[34] Appelbaum J. The role of view factors in solar photovoltaic fields. Renew Sustain Energy Rev 2018;81:161–71.
[35] Ernst M, Conechado GEJ, Asselineau C-A. Accelerating the simulation of annual bifacial illumination of real photovoltaic systems with ray tracing. iScience 2022;25:103698.
[36] Raina G, Vijay R, Sinha S. Study on the optimum orientation of bifacial photovoltaic module. Int J Energy Res 2022;46(4):4247–66.
[37] Rodriguez-Pastor DA, Ildefonso-Sanchez AF, Soltero VM, Peralta ME, Chacartegui R. A new predictive model for the design and evaluation of bifacial photovoltaic plants under the influence of vegetation soils. J Clean Prod 2023;385:135701.
[38] Baricchio M, Korevaar M, Babal P, Ziar H. Modelling of bifacial photovoltaic farms to evaluate the profitability of East/West vertical configuration. Sol Energy 2024;272:112457.
[39] Ineichen P, Guisan O, Perez R. Ground-reflected radiation and albedo. Sol Energy 1990;44:207–14.
[40] Qiao C, Liu S, Huo J, Mu X, Wang P, Jia S, et al. Retrievals of precipitable water vapor and aerosol optical depth from direct sun measurements with EK MS711 and MS712 spectroradiometers. Atmos Meas Tech 2023;16:1539–49.
[41] Khoo YS, Nobre A, Malhotra R, Yang D, Ruther R, Reindll T, et al. Optimal orientation and tilt angle for maximizing in-plane solar irradiation for PV applications in Singapore. IEEE J Photovoltaics 2014;4:647–53.
[42] Pérez R, Seals R, Ineichen P, Stewart R, Menicucci D. A new simplified version of the Perez diffuse irradiance model for titled surface. Sol Energy 1987;39:221–31.
[43] Hottel HC, Sarofim AF. Radiative transfer. New York: McGraw-Hill Book Company; 1967. p. 31–9.
[44] Martin N, Ruiz JM. Calculation of the PV modules angular losses under field conditions by means of an analytical model. Sol Energy Mater Sol Cells 2001;70(1):25–38.
[45] Saliba M, Etgar L. Current density mismatch in perovskite solar cells. ACS Energy Lett 2020;5(9):2886–8.
[46] Li D, Chen JM, Zhang X, Yan Y, Zhu J, Zheng H, et al. Improved estimation of leaf chlorophyll content of row crops from canopy reflectance spectra through minimizing canopy structural effects and optimizing off-noon observation time. Remote Sens Environ 2020;248:111985.
[47] Li H, Yang G, Long H, Feng H, Xu B, Zhao C. Estimating characteristic coefficient of vertical leaf nitrogen profile within wheat canopy from spectral reflectance. Comput Electron Agric 2023;206:107652.
[48] Grzybowski M, Wijewardane NK, Atefi A, Ge Y, Schnable JC. Hyperspectral reflectance-based phenotyping for quantitative genetics in crops: progress and challenges. Plant Commun 2021;2:100209.
[49] Demain C, Journée M, Bertrand C. Evaluation of different models to estimate the global solar radiation on inclined surfaces. Renew Energy 2013;50:710–21.
[50] Lindsay N, Libois Q, Badosa J, Migan-Dubois A, Bourdin V. Errors in PV power modelling due to the lack and angular details of solar irradiance inputs. Sol Energy 2020;197:266–78.
[51] Hassan MA, Akoush BM, Abubakr M, Campana PE, Khalil A. High-resolution estimates of diffuse fraction based on dynamic definitions of sky conditions. Renew Energy 2021;169:641–59.
[52] Monokroussos C, Gao Q, Zhang X, Lee E, Wang Y, Zou C, et al. Rear-side spectral irradiance at 1 sun and application to bifacial module power rating. Prog Photovolt Res Appl 2020;28:755–66.
[53] Dirnberger D, Blackburn G, Müller B, Reise C. On the impact of solar spectral irradiance on the yield of different PV technologies. Sol Energy Mater Sol Cells 2015;132:431–42.
[54] Li Y, Yin G, Schmid M. Bifacial semi-transparent ultra-thin Cu(In, Ga)S_e2 solar cells on ITO substrate: how ITO thickness and Na doping influence the performance. Sol Energy Mater Sol Cells 2022;234:111431.
[55] Cetinkaya C. Efficient and high-bifacial CdTe-based solar cell enabled by functional designed dielectric/metal/dielectric transparent top contact via light management engineering. Opt Mater 2022;133:113003.
[56] Cho J-S, Seo YH, Choi B-H, Cho A, Lee A, Shin MJ, et al. Energy harvesting performance of bifacial and semitransparent amorphous silicon thin-film solar cells with front and rear transparent conducting oxide contacts. Sol Energy Mater Sol Cells 2019;202:110078.
[57] Luque A, Hegedus S. Handbook of Photovoltaic Science and Engineering. John Wiley & Sons; 2011.